

Impact of zigzag tape on blade loads and aerodynamic wake in a vertical axis wind turbine

A Delft VAWT case study

Rogowski, Krzysztof; Michna, Jan; Mikkelsen, Robert Flemming; Ferreira, Carlos Simao

DOI

[10.1016/j.energy.2025.135344](https://doi.org/10.1016/j.energy.2025.135344)

Publication date

2025

Document Version

Final published version

Published in

Energy

Citation (APA)

Rogowski, K., Michna, J., Mikkelsen, R. F., & Ferreira, C. S. (2025). Impact of zigzag tape on blade loads and aerodynamic wake in a vertical axis wind turbine: A Delft VAWT case study. *Energy*, 321, Article 135344. <https://doi.org/10.1016/j.energy.2025.135344>

Important note

To cite this publication, please use the final published version (if applicable). Please check the document version above.

Copyright

Other than for strictly personal use, it is not permitted to download, forward or distribute the text or part of it, without the consent of the author(s) and/or copyright holder(s), unless the work is under an open content license such as Creative Commons.

Takedown policy

Please contact us and provide details if you believe this document breaches copyrights. We will remove access to the work immediately and investigate your claim.



Impact of zigzag tape on blade loads and aerodynamic wake in a vertical axis wind turbine: A Delft VAWT case study

Krzysztof Rogowski ^a, Jan Michna ^a, Robert Flemming Mikkelsen ^b, Carlos Simao Ferreira ^c

^a Institute of Aeronautics and Applied Mechanics, Warsaw University of Technology, Nowowiejska 24, Warsaw, 00-665, Poland

^b Department of Wind and Energy Systems, Technical University of Denmark, Kgs. Lyngby, DK-2800, Denmark

^c Faculty of Aerospace Engineering, Delft University of Technology, Kluyverweg 1, 2629 HS Delft, The Netherlands

ARTICLE INFO

Keywords:

Zigzag tape
VAWT
Actuator line model
URANS
Aerodynamic wake

ABSTRACT

This study investigates the impact of zigzag tape on the aerodynamic performance and wake characteristics of the Delft Vertical Axis Wind Turbine (VAWT). The primary aim is to understand how the zigzag tape affects blade loads and the resulting aerodynamic wake. A comprehensive analysis was conducted using the Actuator Line Model (ALM) with airfoil characteristics measured in the wind tunnel at the Technical University of Denmark (DTU). Additionally, a 2-D CFD analysis with $k-\omega$ SST and γ - Re_θ turbulence models were employed to evaluate the influence of laminar transition phenomena on rotor characteristics. Results indicate that while the zigzag tape linearizes the lift coefficient characteristic, it leads to a notable reduction in aerodynamic efficiency due to increased drag and decreased lift below the critical angle of attack. The simulations were performed at a tip-speed ratio (TSR) of 4.5 to avoid a dynamic stall, as this operating condition ensures that the rotor blades remain below the static stall threshold and large offshore VAWTs are designed to operate near their maximum aerodynamic efficiency (C_p) for the majority of their operational time. The aerodynamic wake behind the rotor also shows significant changes, with the zigzag tape promoting asymmetry and affecting the wake recovery distance. The study's findings highlight the importance of considering surface contamination effects, represented by zigzag tape, in evaluating VAWT performance and wake behavior, offering valuable insights for wind turbine design and optimization.

1. Introduction

In 2015, Tescione et al. [1] conducted extensive experimental studies on a 2-bladed H-shaped VAWT at Delft University of Technology, using Particle Image Velocimetry (PIV) in the Open Jet Facility (OJF). The turbine, featuring NACA0018 aluminum blades, had a height and rotor diameter of 1 m, with a chord length of 0.06 m. The blades were mounted at a point 0.4c from the leading edge. Operating at a free stream velocity of 9.3 m/s, it achieved a tip speed ratio of 4.5.

Since 2015, numerous numerical analyses of this rotor have been conducted. Rotors based on this geometry have been studied using the classical 2-D CFD approach with various boundary layer modeling methods [2–5] and more advanced three-dimensional unsteady Reynolds-averaged Navier–Stokes (URANS) equations [6]. While 3-D CFD, particularly URANS, provides valuable insights into complex flow phenomena such as tip vortices and dynamic stall, its high computational cost remains a limitation. Therefore, lower-order models such as blade element momentum (BEM) and actuator line model (ALM) remain popular alternatives [7]. These methods rely on airfoil aerodynamic characteristics and additional corrections (e.g., flow curvature,

dynamic stall models) and can incorporate finite blade and added mass effects [8].

The aerodynamics of a VAWT rotor are complex and challenging to estimate, leading to significant differences in the aerodynamic characteristics estimated by various researchers [9]. This variability arises from the different modeling approaches employed, including numerical methods such as computational fluid dynamics (CFD), as well as lower-order models such as blade element momentum (BEM) and vortex models, in addition to the inherent sensitivity of the NACA0018 airfoil to operating conditions. For this turbine, the chord-based Reynolds number Re_c at a TSR of 4.5 is approximately 1.7×10^5 [10]. In the “low Reynolds number” range (10^3 to 10^5), viscous effects, laminar separation bubbles, and turbulence play a significant role [11]. According to Winslow et al. [12], at low Reynolds numbers, the boundary layer remains laminar over a larger portion of the airfoil surface, making it more susceptible to separation due to an adverse pressure gradient. The separated shear layer may transition to turbulence and reattach, forming a laminar separation bubble (LSB). However, as the Reynolds

* Corresponding author.

E-mail address: krzysztof.rogowski@pw.edu.pl (K. Rogowski).

number decreases, the reattachment point moves further downstream, increasing bubble size and drag while reducing lift efficiency. In the range of $10^4 < Re < 5 \times 10^4$, the shear layer often does not reattach, leading to trailing edge stall and significantly degraded aerodynamic performance. The NACA0018 profile, common in VAWT design, was not examined under low Reynolds number conditions in a wind tunnel until recently. Early studies, such as those of Jacobs and Sherman (J&S) [13], were limited and influenced by high levels of wind tunnel turbulence. The widely used database by Sheldahl and Klimas (S&K) published in 1971 [14,15] was dominant for a long time, but recent wind tunnel studies and numerical tools such as XFOIL and CFD have provided more accurate data [16–18]. Modern measurements of C_L and C_D at around $Re = 150k$ differ significantly from the S&K and J&S data, showing that flow around a clean profile at sub-critical angles is dominated by laminar bubbles. This causes the $C_L(\alpha)$ curve to follow two different derivatives rather than one. Gerakopoulos et al. [19] identified the point that separates these two regions. Contemporary studies indicate that advanced transition models, such as $\gamma - Re_\theta$ and e^N methods, often misestimate this region without calibration [20]. The aerodynamic characteristics of the NACA0018 profile, as in most airfoils, are sensitive to variations in the Reynolds number. However, in the case of the NACA0018 airfoil, which is often used in VAWT applications, this sensitivity becomes particularly critical due to the low Reynolds number regime in which these turbines are typically operated [20,21].

An effective method to influence the behavior of the boundary layer in experimental aerodynamics is the use of zigzag tape. In the TU Delft VAWT experiment (Fig. 1), zigzag tape was applied at the length of the 8% chord on both sides of the blades to mitigate laminar separation bubbles. The tape, a 3D-turbulator by Glasfaser Flugzeug, had a point distance of 6 mm, was 0.20 mm thick, 12 mm wide, and followed a zigzag pattern of 60° [1]. In addition to promoting transition, zigzag tape is commonly used in experiments to improve control over the aerodynamic characteristics of an airfoil by modifying the behavior of the boundary layer and reducing the influence of laminar separation bubbles [22], as well as mitigating aerodynamic noise [23].

The primary tool used to investigate the impact of zigzag tape on VAWT aerodynamics in this paper is the Actuator Line Model (ALM). To further verify these results and understand the impact of transition phenomena, such as laminar separation bubbles, a 2-D CFD analysis was also performed using the $k-\omega$ SST and $\gamma-Re_\theta$ models. These models have been shown to predict rotor loads accurately [4,24]. The $k-\omega$ SST model is a turbulence model that assumes a fully turbulent flow throughout the boundary layer, providing robust and reliable predictions, particularly in regions with strong adverse pressure gradients. It

has also been used successfully to approximate the effect of zigzag tape by enforcing the early transition [22]. In contrast, the $\gamma-Re_\theta$ model is a transition model that explicitly accounts for the laminar-to-turbulent transition, making it more suitable for capturing transitional effects such as laminar separation bubbles and their influence on aerodynamic loads. This distinction is particularly relevant when analyzing flow conditions at low Reynolds numbers, where transition plays a critical role. Similarly, Kruse et al. [25] studied the aerodynamic characteristics of the NACA 63₃-418 airfoil, demonstrating the significance of surface roughness and transition modeling. Therefore, verifying whether the $k-\omega$ SST model's rotor blade loads match the zigzag tape trend provides further justification for its use in our simulations.

Our analyses revealed several important issues for understanding the relationship between airfoil aerodynamic characteristics and rotor wake. Firstly, in addition to the significant impact on aerodynamic blade loads, the zigzag tape also affects the wake downstream of the rotor—an effect not previously considered for VAWTs but crucial for analyzing the influence of dirty blades on wake geometry. Additionally, using the S&K database results in notable differences in velocity profiles compared to clean airfoils.

This paper has two main parts. The first part presents the aerodynamic characteristics of the clean NACA0018 airfoil and the zigzag tape airfoil, measured at the Technical University of Denmark (DTU). Comparison of the obtained C_L and C_D with XFOIL and the complete 2-D CFD results. The second part discusses VAWT aerodynamic characteristics using the 3-D ALM approach, including a 2-D CFD analysis to understand the impact of laminar transition effects on aerodynamic loads and wake.

2. Experimental setup and wind tunnel testing

The blade model used for wind tunnel tests to determine aerodynamic characteristics C_L and C_D was crafted from a section of a wind turbine blade, as shown in Fig. 2. The blade is an extruded aluminum wing with a NACA0018 airfoil profile. The chord and length of the rectangular wing section were 60 mm and 500 mm, respectively. The airfoil surface was smooth and polished using 800-grit sandpaper to ensure minimal surface roughness.

The dimensions of the wind tunnel test section are $H \times W \times L = 0.5 \text{ m} \times 0.75 \text{ m} \times 2.0 \text{ m}$ with a contraction ratio of 8.5, which provides a very low turbulence intensity ($TI < 0.1\%$) of the mean flow, ensuring that natural transition processes can develop. The maximum velocity achievable in the tunnel is 40 m/s. Measurements were conducted with a sampling rate of 125 Hz for 10 s at each angle of attack (α). Pressure scanners from Pressure Systems were used, having a full range of

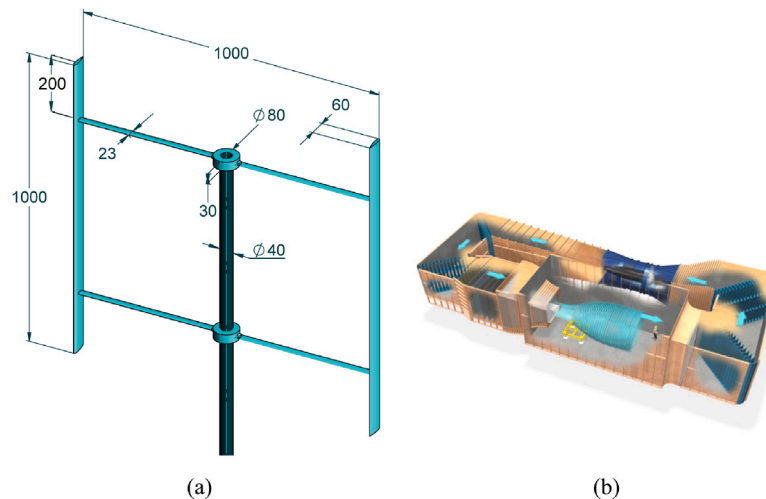


Fig. 1. The VAWT model (dimensions in mm) (a); Schematics of the Open Jet Facility (OJF) [1] (b).

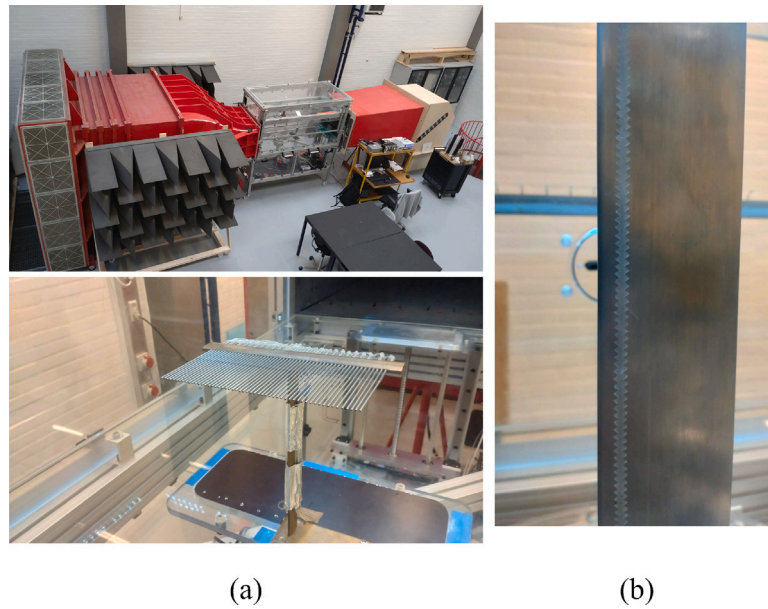


Fig. 2. Experiment equipment and blade configuration.

± 2.5 kPa for wall pressures and ± 7 kPa for wake pressures. Aerodynamic forces were measured using force gauges, wall pressure measurements, and wake pressure readings for the drag. The lift measurements from the force gauge and wall pressures showed good agreement. However, wake measurements are reliable only for $\alpha < \pm 20$ degrees; at higher angles of attack, the wake becomes too wide for the rake used. Also, the airfoil exhibited tonal noise around an angle of attack of 0 degrees.

The baseline aerodynamic characteristics of the clean NACA0018 airfoil were presented in detail in [26], where the discussion of the experimental setup and fundamental data was provided. Due to space limitations, this article does not repeat those details. Instead, it focuses on entirely new results concerning the influence of zigzag tape on the aerodynamic performance of the airfoil.

2.1. Impact of Zigzag tape on NACA0018 airfoil performance

The main goal of the experimental part was to obtain the $C_L(\alpha)$ and $C_D(\alpha)$ characteristics of the NACA0018 airfoil for a Reynolds number as close as possible to the chord-based value, which for the considered 1-m VAWT at TSR=4.5 is 1.7×10^5 . Taking into account the chord length of the airfoil (6 cm) and the maximum flow speed in the wind tunnel (40 m/s), we obtained a Reynolds number of 1.6×10^5 . In our previous work [26], we presented the characteristics of the NACA0018 airfoil for a range of Reynolds numbers from 0.3×10^5 to 1.6×10^5 . The aerodynamic forces that were obtained were validated based on experimental studies by other authors and compared with the predictions of the XFOIL approach. This work discusses the impact of zigzag tape on the airfoil polars.

Fig. 3 shows the performance of the NACA0018 airfoil with zigzag tape; the lift and drag coefficients, C_{Lg} , C_L , and C_D , were estimated using a gauge, wall pressure taps, and a wake rake, respectively. These aerodynamic force characteristics as a function of the angle of attack, shown in this figure, were obtained for $Re = 1.6 \times 10^5$ in the range from -20° to 20° , and then back to -20° to obtain a complete aerodynamic hysteresis loop. Two independent measurement techniques, pressure taps, and force gauge, showed very similar lift coefficients. During the “upward” measurement, the maximum lift coefficient, C_{Lmax} , reached 1.02 at a critical angle of attack of 14° . The lift for the same angle of

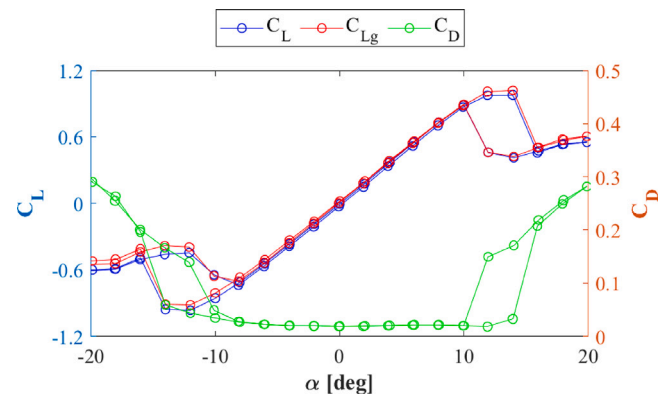


Fig. 3. Experimental Lift Coefficient (C_L) using wall pressure taps and a force gauge (C_{Lg}) as well as Drag Coefficient (C_D) Variation with Angle of Attack (α) for zigzag Configuration.

attack during the “downward” measurement decreased by 58.3%. The C_{Lmax} during the “downward” measurement was 0.88 at an angle of attack of 10° . A relatively large hysteresis loop is also visible in the drag coefficient. The minimum drag coefficient, C_{Dmin} , was 0.019. The tape causes the lift coefficient to grow almost linearly for angles of attack up to α_{crit} at such low Reynolds numbers, with the derivative $dC_L/d\alpha$ equal to 4.87 rad^{-1} .

A comparison of the obtained characteristics for the airfoil with zigzag tape (Fig. 3) and the clean airfoil configuration is presented in Fig. 4. The $C_L(\alpha)$ characteristics of the clean airfoil are nonlinear below α_{crit} , which is due to the presence of laminar bubbles that form on both sides of the airfoil up to the transition angle α_t of approximately 6° – 7° , or only on the pressure side beyond α_t [19,20]. Applying the zigzag tape induces turbulence in the boundary layer, eliminating this effect. Interestingly, despite removing laminar bubbles, the hysteresis loops

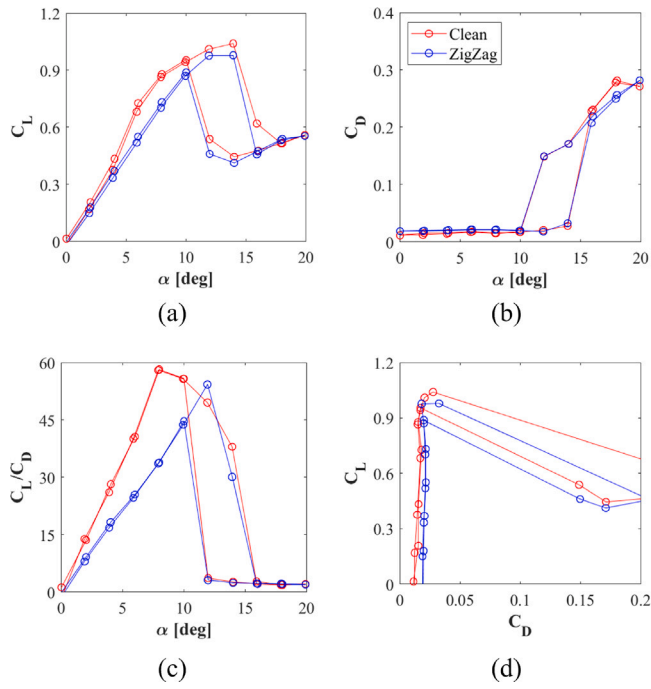


Fig. 4. Comparison of aerodynamic performance for the NACA0018 airfoil: (a) lift coefficient C_L vs. angle of attack α , (b) drag coefficient C_D , (c) lift-to-drag ratio C_L/C_D , and (d) C_L vs. C_D . Results are shown for both clean [26] and zigzag tape configurations.

for both the clean airfoil and the airfoil with zigzag tape remain quite similar in terms of value and shape. However, the presence of the tape increases the minimum drag by approximately 73.4%. The nonlinearity of the $C_L(\alpha)$ curve leads to a significant improvement in aerodynamic efficiency (Fig. 4c).

2.2. The effect of Reynolds number on the performance of NACA0018 airfoil with zigzag tape

The results given in Fig. 5 are compared for Reynolds numbers 0.83×10^5 and 1.60×10^5 . This comparison aims to highlight the zigzag tape's significant impact on the airfoil characteristics, especially within the range of such low Reynolds numbers. As shown in Fig. 5a, the zigzag tape linearizes the C_L characteristics, resulting in very similar $dC_L/d\alpha$ derivatives for both Reynolds numbers. The derivatives of both characteristics, calculated in the range from 0° to 10° , have an average value of 4.87 rad^{-1} . This value is 22.5% lower compared to the theoretical derivative of 2π of a thin airfoil as predicted by Thin Airfoil Theory [18]. As mentioned earlier in the previous subsection, two regions can be distinguished for the clean airfoil characteristics: in the first region, laminar separation bubbles occur on both sides of the airfoil, while in the second, they appear only on the suction side. Gerakopoulos et al. [19] demonstrated that for $Re = 0.8 \times 10^5$, the derivative in the angle of attack range $0^\circ \leq \alpha \leq 6^\circ$ is 0.14, while in the range $6^\circ \leq \alpha \leq 10^\circ$, it is 0.03. In our measurements, the transition angle α_t occurred slightly earlier, at approximately 4° , with aerodynamic derivatives for the first and second regions being 0.145 and 0.056, respectively. For $Re = 1.6 \times 10^5$, Gerakopoulos et al. [19] obtained derivatives for the first region ($0^\circ \leq \alpha \leq 8^\circ$) of 0.11 and for the second region ($8^\circ \leq \alpha \leq 14^\circ$) of 0.02. Our predictions are 0.108 for the first region ($0^\circ \leq \alpha \leq 8^\circ$) and 0.027 for the second region ($8^\circ \leq \alpha \leq 14^\circ$).

Moreover, the Reynolds number significantly affects C_{Lmax} , with the observed differences becoming more pronounced as the Reynolds number decreases. This effect is particularly evident in the case of the clean configuration, where the lack of surface modifications leads to

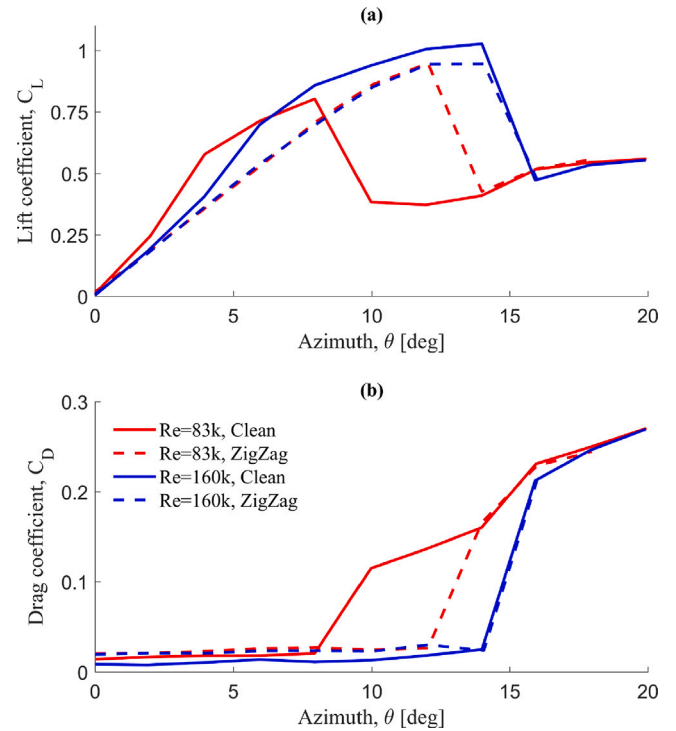


Fig. 5. Comparison of the lift coefficient C_L (a) and drag coefficient C_D (b) for the zigzag configuration of the NACA0018 airfoil, with clean airfoil data from [26], across three Reynolds numbers ($Re = 83k$ and $Re = 160k$) for angles of attack ranging from 0° to 20° .

greater sensitivity to flow separation and boundary layer behavior at lower Reynolds numbers. The C_{Lmax} for the lowest examined Re is 0.8 at $\alpha = 8^\circ$ for the clean airfoil and 0.94 at $\alpha = 12^\circ$ for the zigzag configuration. When comparing these results to other studies, specifically for the clean airfoil case, as no similar investigations involving zigzag tape are known to the authors of this paper, Gerakopoulos et al. [19] reported a C_{Lmax} of 0.88 at $\alpha = 10^\circ$ for $Re = 0.8 \times 10^5$, and 1.02 at $\alpha = 14^\circ$ for $Re = 1.6 \times 10^5$. For the higher Reynolds number of $Re = 1.6 \times 10^5$, the differences in C_{Lmax} between the clean and zigzag configurations are relatively small. The C_{Lmax} for the clean configuration is 1.027, which is 8% lower compared to the zigzag configuration. For $Re = 1.6 \times 10^5$, the critical angle of attack α_{crit} is 14° . This analysis demonstrates that the measurement results presented in this paper are acceptable. The differences between our results and those taken from the literature increase as the Reynolds number decreases, and these differences are influenced by the conditions in the wind tunnel and the measurement tools used.

The Reynolds number also significantly affects the drag coefficient (Fig. 5b). The clean airfoil's minimum drag coefficient strongly depends on the Reynolds number. As shown in [26], C_{Dmin} increased from 0.0084 for $Re = 1.6 \times 10^5$ to 0.014 for $Re = 0.83 \times 10^5$, that is, by 65.5%. The zigzag tape, however, causes the drag coefficient to increase more slowly, from 0.0195 for $Re = 1.6 \times 10^5$ to 0.0196 for $Re = 0.83 \times 10^5$. The increase in the angle of attack first causes a slight increase in drag, followed by a sharp increase. Both the Reynolds number and the zigzag tape significantly affect the angle of attack at which this sharp increase in drag occurs. For $Re = 0.83 \times 10^5$, this sharp increase appears in $\alpha = 7.95^\circ$ for clean airfoil and 12.04° for zigzag tape. For the highest Reynolds number studied in this work, a sharp increase in drag is observed at the same angle of attack.

3. Methodology

3.1. Actuator line approach

The three-dimensional Actuator Line Model (ALM), developed by Sørensen and Shen [27], combines classical blade element theory with Navier–Stokes-based flow models. This study uses the turbinesFoam library by Bachant et al. [28] within the OpenFOAM CFD framework, significantly reducing computational costs compared to RANS simulations solved with 3D blades.

The ALM represents wind turbine blades as lines of actuator elements at their quarter-chord position, using 2-D airfoil lift and drag coefficients. Blade forces are calculated from local velocities using the angle of attack and relative velocity for each blade element. The blade element method couples with a modified Leishman–Beddoes dynamic stall model [29–31] to determine dynamic blade force coefficients. The calculated body forces are reintroduced into the Navier–Stokes solver as momentum equation terms.

The relative flow velocity and angle of attack for each blade element are computed using the vector sum of the tangential velocity V_t and the local inflow velocity U_{in} . The tangential velocity $V_t = -\omega R$ is determined by the rotor angular velocity ω and the rotor radius R , while U_{in} is obtained from the surrounding flow field at the position of the quarter-chord of the blade element. In OpenFOAM, the `interpolationCellPoint` class is used for linearly weighted interpolation of cell values, ensuring smooth sampling of U_{in} . According to Mendoza et al. [32], this approach mitigates abrupt velocity variations caused by mesh resolution, particularly when the mesh size is comparable to the chord length and blade elements traverse approximately one cell per time step.

Prandtl's lifting line theory is applied in the ALM to account for the blade's end effects. The geometric angle of attack is expressed as a function of the non-dimensional span position, allowing for the determination of unknown Fourier coefficients that describe the circulation distribution along the span. These coefficients are then used to adjust the lift coefficient distribution, ensuring consistency with the physical effects of blade-tip vortices. Based on the normalized spanwise lift coefficient distribution, the correction function is incorporated into the ALM to model the lift force variations near the blade tips accurately.

In this study, dynamic effects on lift and drag are taken into account using the Dynamic Stall Model (DSM), which ensures proper aerodynamic modeling in different operating conditions. These effects are characterized by the reduced frequency $k = \frac{TSR \cdot c}{2R}$, where k depends on the tip speed ratio (TSR), the length of the blade chord c , and the radius of the rotor R . For the turbine examined in this manuscript, at $TSR = 4.5$, the reduced frequency is 0.27, matching the conditions of an experimental turbine studied by Bachant et al. [33]. Although the range of attack angles experienced by the turbine blades in this study did not exceed critical static stall angles, rendering the dynamic stall effects negligible [7], the DSM was still implemented consistently [32] to ensure robustness and accuracy in aerodynamic modeling.

Based on Mendoza et al. [7], who investigated various Large Eddy Simulation (LES) approaches (including Smagorinsky, dynamic k -equation, and dynamic Lagrangian turbulence models) and found minimal differences, the Smagorinsky LES approach was used in this study to calculate the velocity field. A detailed description of the ALM methodology and additional models is available in Bachant et al. [33]. The Navier–Stokes equations for incompressible flow are solved using the Pressure-Implicit with Splitting of Operators (PISO) algorithm [34].

The TU Delft VAWT (Fig. 1) simulated in this study is based on the geometry of Tescione et al. [1], with the struts and supporting towers excluded for simplicity. The simulation domain (Fig. 6) was set to 20D to examine the wake at a greater distance behind the rotor.

The uniform distribution of hexahedral cells was used near the turbine rotor, with a local refinement level of $n = 4$, gradually transitioning to a coarser mesh further from the rotor to accurately capture the

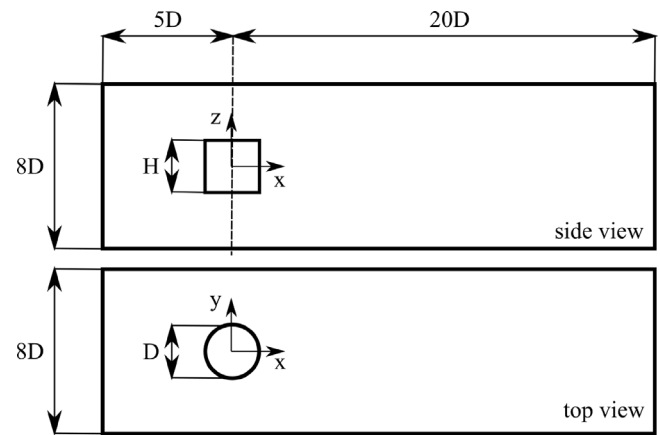


Fig. 6. Schematic of the numerical simulation domain for the TU Delft VAWT for the ALM approach.

details of the wake (Fig. 7). This topology remained consistent and was globally refined, with the mesh scaled proportionally in all directions. The finest refinement region extends $1D$ upwind and $11D$ downwind from the central shaft, covering $1D$ horizontally and vertically from the equatorial blade section.

Fig. 8 compares the power coefficient c_p for the entire rotor at three mesh resolutions: $D/60$, $D/80$, and $D/96$. Although small differences in the curves can be observed, particularly for finer mesh resolutions, these differences remain minor and are natural in the case of the applied LES approach, where finer meshes capture more detailed flow structures. This observation is consistent with the findings of Mendoza et al. [7], who showed that increasing mesh density within the range of $D/40$ to $D/96$ leads to minor changes in aerodynamic wake profiles. However, these changes remain at the flow details level and do not significantly impact the velocity profiles behind the rotor, which could influence the power characteristics of a downstream turbine.

Similar conclusions were drawn by Huang [35], who validated the ALM approach for a similar but slightly smaller rotor with a diameter of 0.3 m. Huang's work, which involved PIV measurements of a significantly longer aerodynamic wake, demonstrated that using the k -epsilon turbulence model provides sufficiently accurate results to estimate the wake deficit, even with less dense computational meshes.

Given the scope of our study, the reference mesh resolution for this work is $D/80$. This resolution offers a practical balance between computational efficiency and accuracy, ensuring reliable predictions of flow characteristics within the rotor aerodynamic wake, which are crucial for assessing the potential placement of downstream wind turbines in a wind farm.

As recommended by Mendoza et al. [7], the maximum Courant number (Co) should be kept below 0.25. In this study, it remained below 0.15.

3.2. 2-D CFD modeling

The 2-D computational domain (Fig. 9) represents the equatorial plane of the TU Delft VAWT with a high blade aspect ratio (H/c) of 16.7 and a zero-pitch angle; therefore, the 3-D tip effects are insignificant [2,36]. The domain width is $W = 25D$, providing a blockage ratio, defined as the ratio of turbine diameter D to domain width W , of 4%. Rezaeiha et al. [37] showed that for CFD simulations of VAWTs, a blockage ratio of less than 5% is necessary to minimize the effect of boundary conditions on the results. The distance from the inlet to the rotor axis was set to $10D$, while the total domain length was $35D$. In the rotor area, a moving ring with an outer diameter of $2D$ and an inner diameter of $0.5D$ was used. The dimensions of our domain meet the

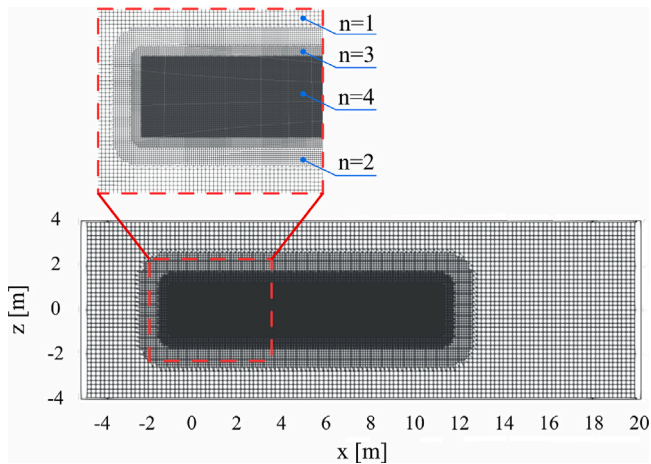


Fig. 7. Mesh for VAWT simulations using the ALM approach. The figure shows the full view of the mesh in the x - z plane with a zoomed-in section illustrating different levels of local refinement: $n = 1$, $n = 2$, $n = 3$, and $n = 4$.

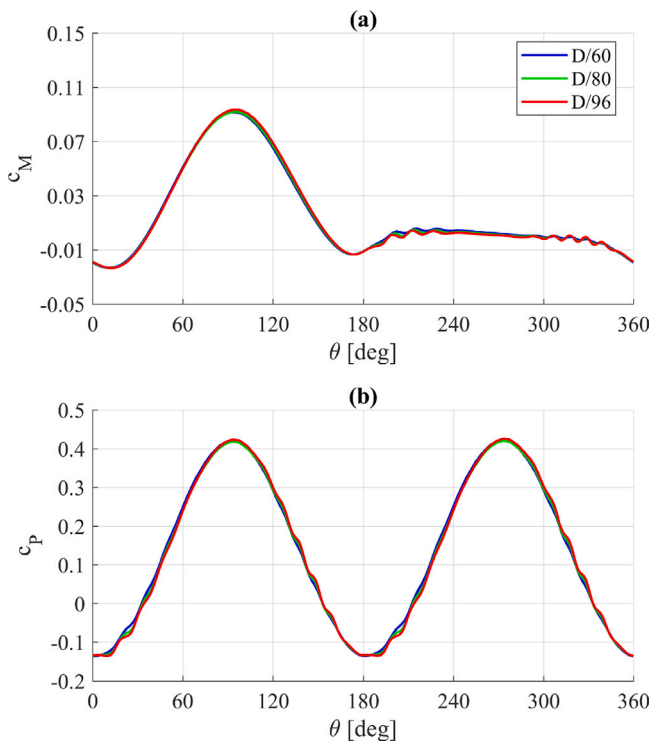


Fig. 8. Comparison of the moment coefficient c_M for a single rotor blade (top) and the power coefficient c_P for the entire rotor (bottom) at three mesh resolutions: $D/60$, $D/80$, and $D/96$.

minimum criteria specified in Rezaeiha et al. [37] for small VAWTs of low solidity that operate at moderate tip speed ratios.

Fig. 9 presents the mesh for the TU Delft VAWT, consisting of quadrilateral mapped elements. Following a grid independence study (Fig. 10) conducted on meshes ranging from 1000 to 2000 nodes on the airfoil edges, a mesh with 1460 nodes and a total of approximately 1,276,000 elements was selected for use. The grid convergence study was conducted using a refinement factor of $\sqrt{2}$. The coarser mesh contained approximately 1,033,000 elements, while the finest mesh comprised 2,104,000 cells.

The boundary conditions applied include a uniform velocity at the inlet, zero gauge pressure at the outlet, no-slip conditions on the airfoils, and symmetry along the domain sides. The rotating ring is

connected to the stationary surrounding domain via a sliding mesh interface. The turbulence intensity (TI) at the inlet was set to 5%, while the turbulence length scale was assumed to be 0.004 m. The turbulence decay is observed, and TI levels before the rotor become 0.25–0.35%, consistent with the estimation formula proposed in the ANSYS Fluent Theory Guide [38]. The turbulence intensity level is consistent with the experiment [1] where the maximum available values of TI are 0.5%.

Fig. 10 presents the results of the instantaneous moment coefficient at the 20th rotor revolution for the three investigated mesh distributions. As can be seen from the figure, the differences between the curves are minimal. Furthermore, the coefficient of determination R^2 of the curves compared to the finest mesh result is greater than 0.9999 for both $N = 1460$ and $N = 1000$ cases.

4. Results and discussion

4.1. Aerodynamic blade loads

Fig. 11 presents the local angle of attack of the TU Delft VAWT blade calculated using the 3-D ALM approach based on the lift and drag characteristics of the NACA0018 airfoil measured in the DTU wind tunnel. The blue curve represents the data for the clean airfoil, while the red curve shows the zigzag tape configuration. For comparison, the figure also displays the angle of attack obtained using the airfoil characteristics from Sheldahl and Klimas [14] (black curve). The blade's angle of attack calculated using this database is almost perfectly in line with the results of Mendoza et al. [7], who also used polars from the S&K database in their work. This confirms that the ALM approach implemented in this study is accurate and reliable.

Figs. 12 and 13 compare the components of the sectional aerodynamic blade load, namely the normal and tangential components, calculated using the 3-D ALM and 2-D full CFD approaches. The angle of attack of the blade and the sectional forces differ slightly from each other. It is essential to clarify that the “sectional angle of attack” refers to the angle of attack calculated locally for the blade element in the equatorial plane based on the velocity components and airfoil characteristics specific to that section. This term differs from the “blade angle of attack”, which represents the angle calculated for the entire blade, assuming uniform flow conditions. In Fig. 11, the local blade angle of attack is compared with the sectional blade angle of attack for the blade element in the equatorial plane. The color scheme of the curves corresponding to the various airfoil characteristics has been preserved, but dashed lines have been used for differentiation. Fig. 11 shows that, particularly in the upwind part of the rotor, the differences between the $\alpha(\theta)$ curves are small enough that an additional zoomed-in plot Fig. 11b was prepared to capture them. Higher angles of attack are achieved for the S&K database and for the zigzag configuration, which corresponds to linear $C_L(\alpha)$ characteristics. For the zigzag case, the maximum sectional angle of attack is 13.48° at an azimuth of 106° , while for the S&K database, it is 13.46° at an azimuth of 103.3° . In the case of the clean airfoil, the maximum angle of attack is 12.9° at an azimuth of 104.3° . The average sectional maximum angle of attack is 3.22% lower compared to the blade angle of attack.

For the S&K database, the maximum static lift coefficient of the NACA0018 at $Re = 1.6 \times 10^5$ is reached at $\alpha_{crit} = 12^\circ$, meaning that dynamic stall effects are not significant, as also confirmed by Mendoza et al. [7]. For the VAWT blade angle of attack with the measured airfoil characteristics, the static $C_{L,max}$ is never reached for both the clean airfoil and the zigzag configuration, $\alpha_{crit} = 13.92^\circ$ (Fig. 5).

The differences between all curves are also insignificant in the downwind part, although they are slightly larger than in the upwind part. For the azimuth range of $\theta \approx 260^\circ - 280^\circ$, there is a slight deviation in the angle of attack characteristics calculated for the S&K case compared to the results of Mendoza et al. [7]. This discrepancy arises only because the effect of the rotating tower is not considered in our simulations. However, even without accounting for this effect, the

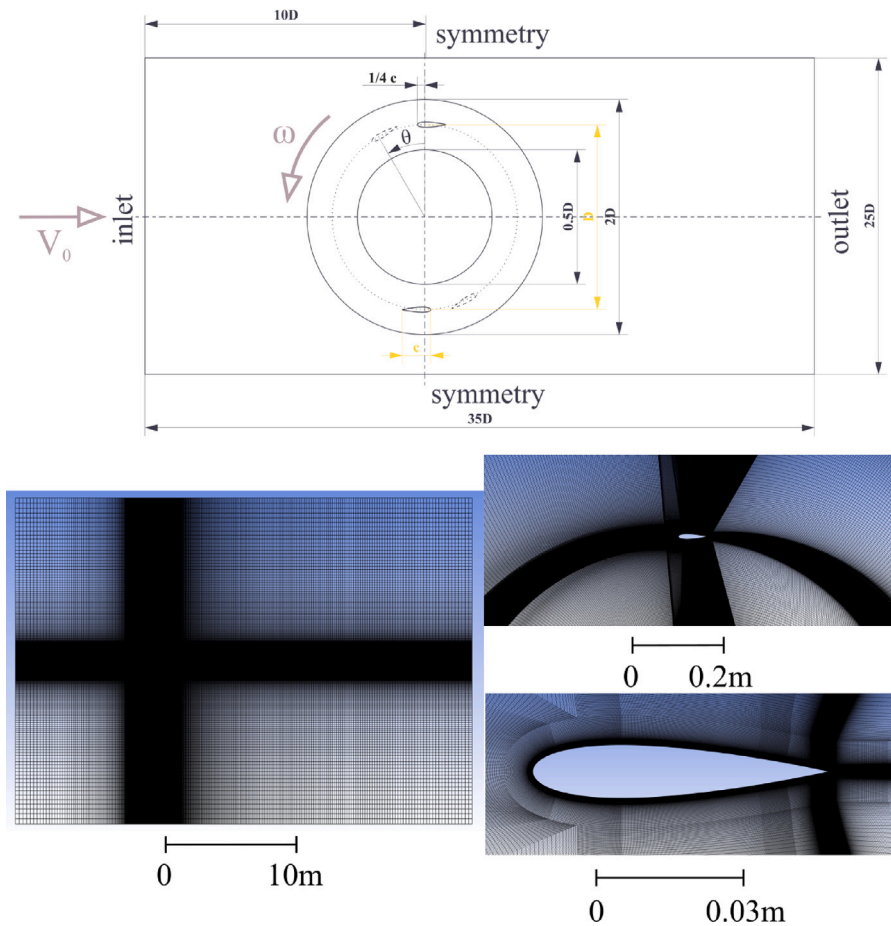


Fig. 9. Computational domain and numerical grid for 2-D CFD simulations. The top scheme illustrates the overall computational domain with boundary conditions and key dimensions. The bottom left image shows a cross-sectional view of the mesh, while the bottom right images provide detailed views of the mesh refinement around the blade.

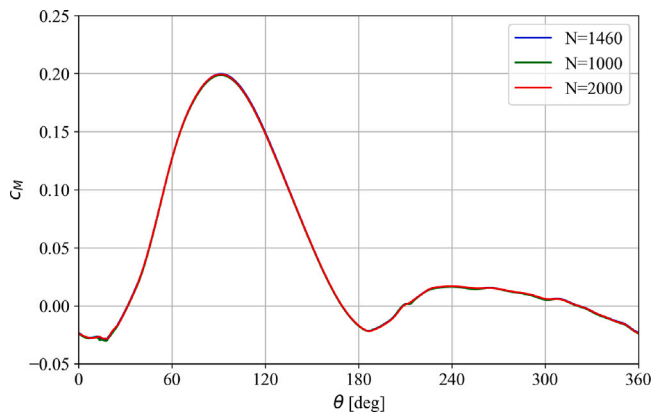


Fig. 10. Instantaneous moment coefficient from 2-D CFD simulations. Mesh sensitivity test. N is the number of nodes on the airfoil edges.

differences between our calculated results and those from the literature are minimal.

The azimuth range corresponding to the largest differences in the angle of attack estimation is $\theta \approx 197^\circ - 300^\circ$. These differences are

caused by the velocity field affected by the blade moving in the upwind part of the rotor and by the airfoil characteristics. The velocity field behind the clean airfoil is more disturbed due to laminar separation bubbles that form on the airfoil surfaces, shed vortices, and evolve in the wake, as also shown in Section 4.2. The differences between the blade and the sectional angle of attack are also more significant than in the upwind part of the rotor.

Since the rotor of the considered TU Delft VAWT operates at a TSR = 4.5, dynamic stall effects are not particularly significant. Therefore, the primary influence on the aerodynamic blade loads, namely the normal and tangential components shown in the non-dimensional form in Figs. 12 and 13, is exerted by the local angle of attack and static airfoil characteristics. The instantaneous sectional loads obtained using the 3-D ALM method and presented in these figures are additionally compared with the 2-D CFD predictions.

It is worth noting that the differences between the 2-D CFD results for the two turbulence models, the $k-\omega$ SST and the $\gamma-Re_\theta$, are minimal, despite the noticeable differences in the static $C_L(\alpha)$ and $C_D(\alpha)$ characteristics generated by both models, as shown in studies by [16,20]. Similar conclusions regarding aerodynamic loads for this 2-D VAWT at TSR = 4.5 examined using SST-based turbulence models can be found in [10]. Determining the local angle of attack using the full 2-D CFD approach is quite challenging. Melani et al. [39], who attempted to determine the local angle of attack for the considered VAWT, concluded that the resulting angle of attack trends showed significant sensitivity to the chosen method, especially in the range of azimuths where the

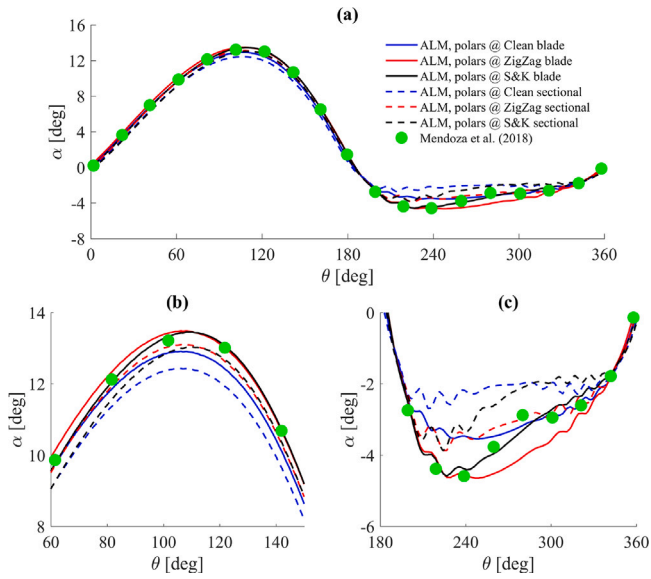


Fig. 11. Local angle of attack characteristics for the TU Delft VAWT. The results obtained by Mendoza et al. [7] using the LES approach are included for comparison.

blade angles of attack reach their maxima. Nevertheless, these authors demonstrated that, depending on the method used, the maximum local blade angle of attack ranges between 8 and 11 degrees. Therefore, the flow should be considered as mostly attached. Furthermore, within the angle of attack range of 8 to 11 degrees, the $C_L(\alpha)$ results obtained with the $k-\omega$ SST model are slightly higher compared to the γ - Re_θ approach, which explains the slight excess in tangential blade loads (Fig. 13). Laminar separation bubble effects captured by the γ - Re_θ model are evident in the aerodynamic load coefficients up to approximately $\theta \approx 80^\circ$. It can be observed that the loads generated by the transition model are slightly greater, with small vortex structures appearing.

It should be emphasized that the differences between the results from the ALM with polars of the clean airfoil (excluding the S&K database) and 2-D CFD are minimal in the upwind part of the rotor, while they are somewhat larger in the downwind part. This results from the two different ways of modeling rotor flow: 3-D ALM and full 2-D CFD. In the downwind part, the 2-D CFD approach has the advantage of determining aerodynamic characteristics by considering local flow conditions. On the other hand, in the ALM approach, airfoil characteristics measured or calculated under low-turbulence conditions are used for the entire rotor revolution. However, the full 2-D CFD does not account for the influence of the third dimension. Huang [35] analyzed the TU Delft VAWT for various aspect ratios (AR) ranging from 1 to 10 (where $AR = H/D$) using the ALM approach. He showed that for $AR = 10$, the 3-D effects are much less significant. Therefore, it can be assumed that the aerodynamic loads in the downwind part of a 3-D rotor will be smaller than suggested by the 2-D CFD model, as also demonstrated by Lam and Peng [6].

The aerodynamic blade loads obtained for airfoil characteristics with zigzag tape differ the most from the others but are qualitatively the closest to the blade loads computed using the S&K database. The differences arise from the balance between the lift and drag coefficients. As shown in the experimental section, the airfoil with the zigzag tape maintains the maximum lift coefficient at the level of the clean airfoil's C_{Lmax} . Still, the lift is significantly lower below the critical angle of attack. Since, as discussed in the paragraph on the local angle of attack, the static critical angle of attack is not exceeded, the rotor blade at $TSR = 4.5$ operates at much lower C_L and simultaneously at higher C_D

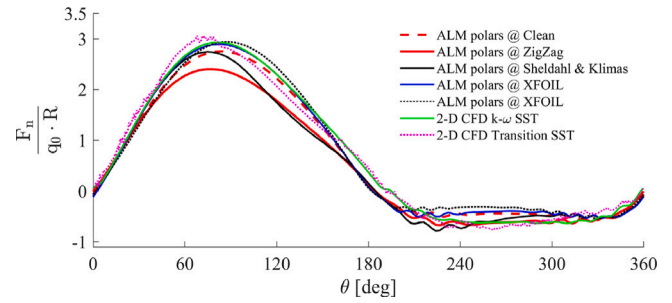


Fig. 12. Comparison of the normal force characteristics for the TU Delft VAWT using different airfoil polars and a 2-D CFD approach.

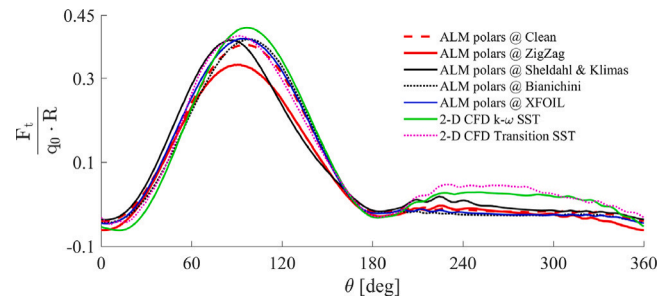


Fig. 13. Comparison of the tangential force characteristics for the TU Delft VAWT using different airfoil polars and a 2-D CFD approach.

than the clean blade. This finding explains the much lower maximum values of the tangential and normal force coefficients than the other characteristics. Due to the similar linear behavior of the lift coefficient in the case of the S&K database, the nature of the aerodynamic loads is similar to that of the zigzag configuration. However, the very low drag coefficients in the case of this database mean that the maximum aerodynamic loads are higher than the zigzag.

There are publications [25] showing that the $k-\omega$ SST turbulence model, treating the entire boundary layer as turbulent, can approximate the effect of zigzag tape or profile contamination to some extent. This particular example shows that the impact of the applied zigzag tape on airfoil performance is significant enough that attempting to model the effect of the tape using the 2-D CFD approach with the $k-\omega$ SST turbulence model yields results that are more similar to those of the clean airfoil.

To contextualize these findings further, it is worth noting that similar observations have been made in previous studies. For example, Mendoza [40] analyzed a 3-bladed 12 kW turbine operating at an optimal TSR of 3.44, comparing results obtained using two independent sources for airfoil polars: XFOIL and the S&K database. Their findings indicated that the C_p curve was significantly underestimated when using S&K data, while XFOIL results led to a slight overestimation. Despite the fact that the rotor diameter in Mendoza's study was more than six times larger than that of the TU Delft VAWT, the normal force results obtained for both polar sources showed qualitative agreement with our findings.

Furthermore, Mendoza [40] noted that the dynamic stall model (DMS) they applied tended to overestimate drag, which consequently led to an underestimation of the tangential force and thus lower C_p values. This aligns with our findings regarding the impact of different polar sources on aerodynamic loads, particularly for the zigzag configuration. These results reinforce the need for further refinements in dynamic stall modeling within the ALM framework to improve simulation accuracy.

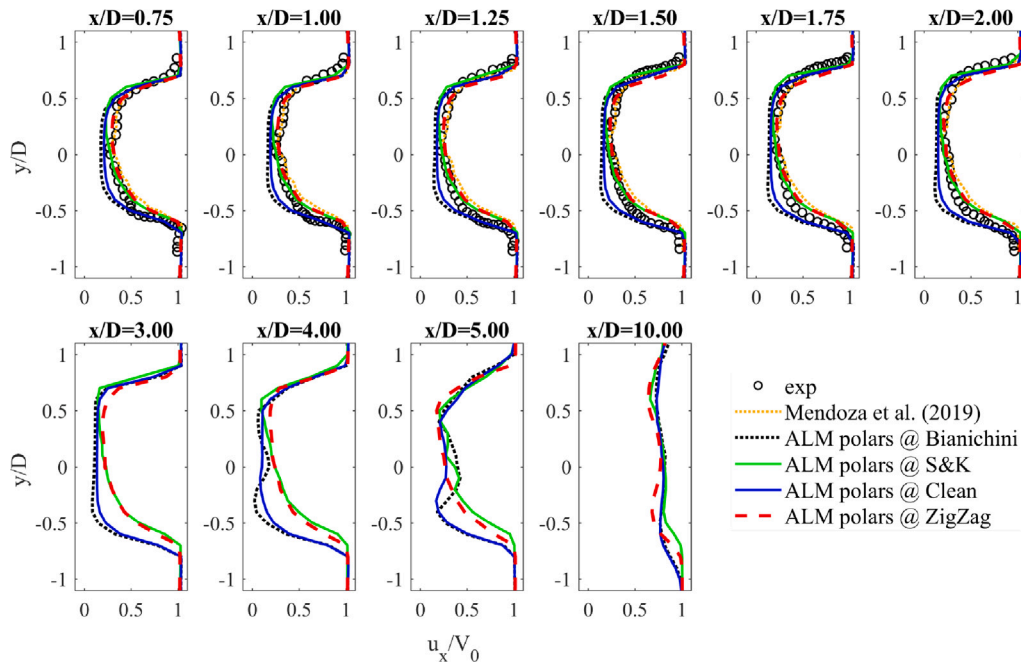


Fig. 14. Comparison of the normalized u_x velocity profiles at various distances x/D downstream of the rotor, obtained using the ALM with experimental results from [1] and velocity profiles from [7].

4.2. Velocity profiles in the aerodynamic wake

Fig. 14 compares the profiles of the average u_x velocity component normalized by the undisturbed flow velocity V_0 at various distances x/D downstream behind the rotor, obtained by the Actuator Line Model. In the experiment, the velocity profiles were recorded up to $x/D = 2.0$. Our paper extends this range to $x/D = 10$ to demonstrate the effect of the zigzag tape on the aerodynamic wake at a distance suitable for installing another wind turbine. For this comparison, we used two sets of polars from our experiment and two from the literature: Bianchini et al. [41] and Sheldahl and Klimas [14]. The velocity profiles from Mendoza et al. [7] were also used for comparison. The figure shows that the velocity profiles using S&K polars, calculated by both this study (green curve) and Mendoza et al. (orange dashed curve), are similar. The minor differences in these profiles are likely due to the influence of the rotating shaft and struts, which were not included in our simulations. This conclusion is supported by Huang et al. [42], who also neglected the struts and supporting towers in their simulations of the TU Delft VAWT. The velocity results show the asymmetry of u_x profiles around $y/D = 0$ for the S&K polars and zigzag tape, compared to the clean profile, which is due to vortex structures generated on the profile with the free transition. Fig. 14 shows that, for a turbine operating in the wake of another, this effect can be significant at $x/D > 1.75$. As shown in Fig. 15, the profile's surface condition has little impact on the lateral velocity component u_y in the wake. However, effects related to laminar bubbles remain noticeable at $x/D = 4$.

Fig. 16 shows the u_x velocity component distributed along lines parallel to the turbine shaft at several x/D positions. The ALM approach with S&K characteristics yields results similar to Mendoza et al. [7]. Up to $x/D = 1.0$, the ALM with both S&K and zigzag tape characteristics closely matches the experimental data. However, accuracy declines as x/D increases, likely due to modeling issues, such as boundary conditions and empirical relationships for a finite-length blade.

4.3. Velocity fields in the wake of a rotor

The previous subsection discussed velocity distributions along selected lines behind the rotor, showing that the zigzag tape increases

wake asymmetry. This section presents instantaneous and averaged velocity fields in the rotor area to highlight further this asymmetry caused by the absence of laminar bubbles. The experiment by Tescione et al. [1] included PIV measurements of the velocity field in the rotor area, with an example of the instantaneous velocity u_x/V_0 shown in Fig. 17. The results of the ALM approach from Mendoza et al. [7] are presented alongside. Fig. 17 compares our ALM-derived velocity field distributions for the clean and zigzag tape configurations. Compared to Mendoza et al. [7], the slightly coarser grid reveals fewer details. For the clean profile, a wide, more symmetrical low-velocity region is visible compared to the zigzag tape results. Fig. 18 essentially shows the same results as Fig. 17, but it covers a much longer area behind the rotor, extending ten rotor diameters. The figure compares the instantaneous velocity u_x/V_0 for the clean profile and zigzag tape. From this perspective, two features are apparent: the aerodynamic wake is wider for the clean profile, and wake recovery occurs later for the zigzag tape profile.

Fig. 17 shows that both turbulence models in our 2-D CFD simulations yield similar results, closely matching those from the zigzag tape and the ALM approach by Mendoza et al. [7] using S&K data.

Fig. 19 provides another view of the velocity field behind the rotor, showing time-averaged streamwise velocity contours at various x/D locations. At $x/D = 10$, the wake recovers faster with S&K data and zigzag tape than with the clean airfoil. Closer positions, up to $x/D \approx 4.0$, reveal a higher velocity region for negative y/D .

5. Conclusions

The research presented in this paper focuses on investigating the impact of zigzag tape on the performance of the TU Delft VAWT and the aerodynamic wake downstream behind it. Numerical studies were conducted using the actuator line model and airfoil characteristics measured in the DTU wind tunnel. The conclusions drawn from this study are as follows:

- The measured aerodynamic characteristics of a rectangular wing with a NACA0018 airfoil, without the use of turbulators, show a strong nonlinearity in the $C_L(\alpha)$ characteristic, resulting from the formation of laminar bubbles on both the suction and pressure

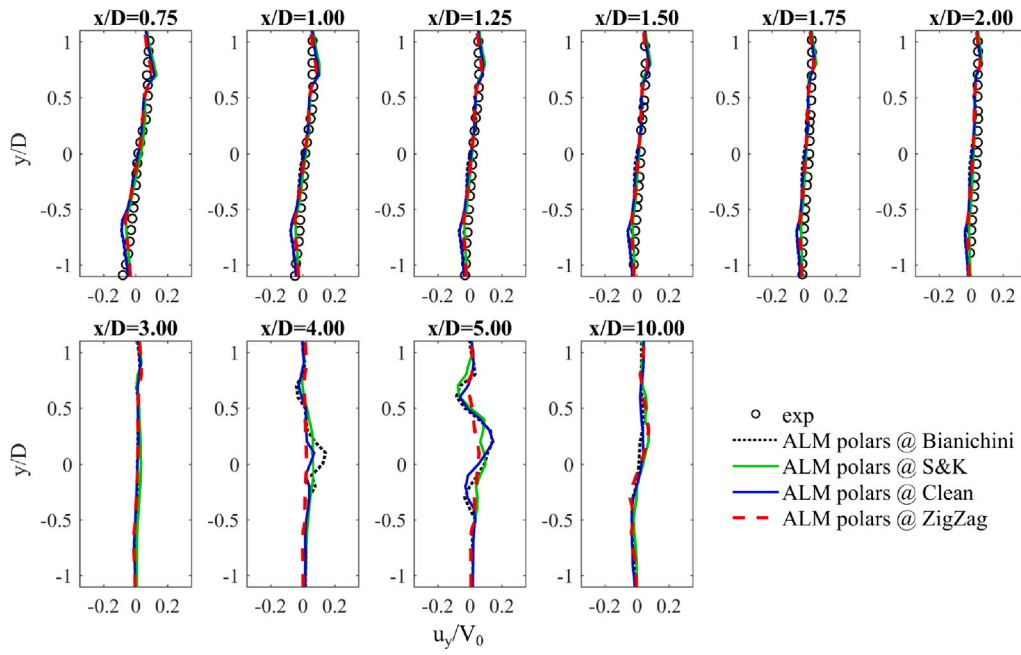


Fig. 15. Comparison of the normalized u_y velocity profiles at various distances x/D downstream of the rotor, obtained using the ALM, with experimental results from [1].

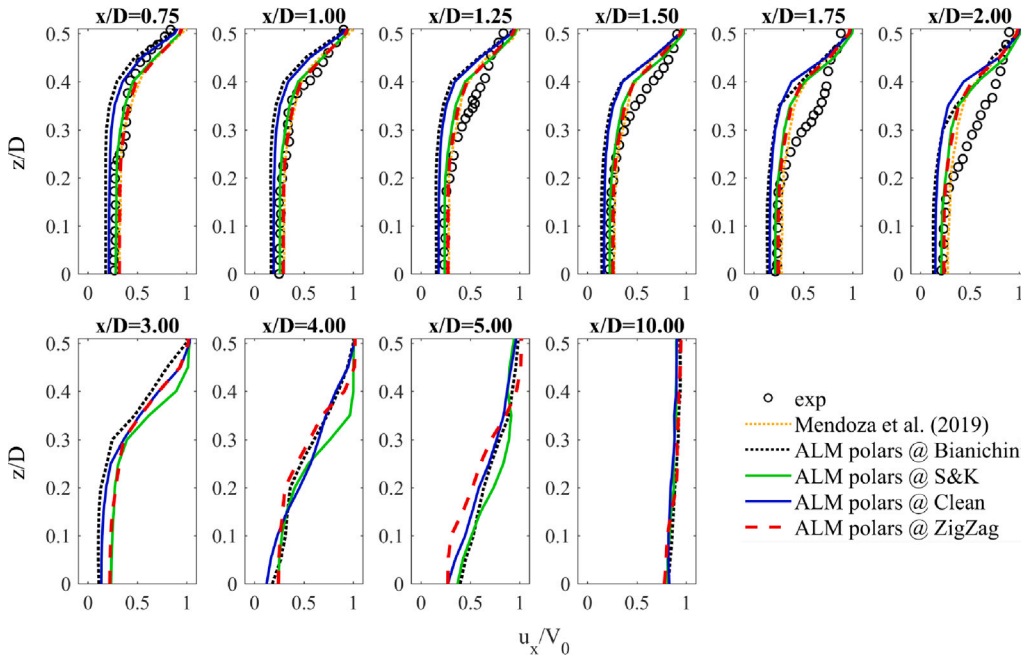


Fig. 16. Comparison of the normalized u_x velocity profiles at various distances x/D downstream of the rotor, obtained using the ALM, with experimental results from [1] and velocity profiles from [7].

sides of the airfoil. This indicates that the selected airfoil performs poorly under these flow conditions, especially at such a low Reynolds number. The application of turbulators allows for the linearization of the lift coefficient characteristic without a significant loss in the maximum C_L value. However, this procedure ultimately leads to a deterioration of the overall aerodynamic characteristics of the rotor, as the lift coefficient values below α_{crit} degrade significantly, and the presence of turbulators generates substantial additional drag.

- The zigzag tape, despite “linearizing” the static lift coefficient characteristic without reducing the maximum lift, significantly lowers the aerodynamic loads on the rotor blades operating at a tip-speed ratio where high aerodynamic efficiency, i.e., a high power coefficient, is expected. It also leads to a substantial change in the wake velocity field behind the rotor.
- The zigzag tape, in addition to controlling flow separation on the airfoil, can also be used to emulate surface contamination caused by factors such as insects, dust, etc. A tape of such a large

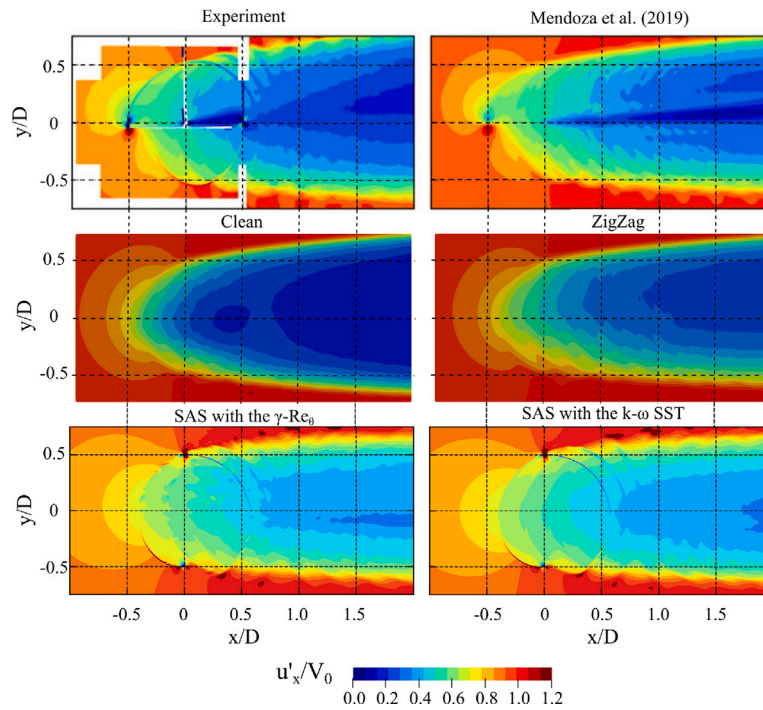


Fig. 17. Contour plots of the normalized instantaneous u'_x/V_0 velocity component in the turbine wake for clean and zigzag tape configurations. The top row compares PIV measurements with the ALM model from [7], the middle row shows velocity distributions for both configurations, and the bottom row presents 2-D CFD results.

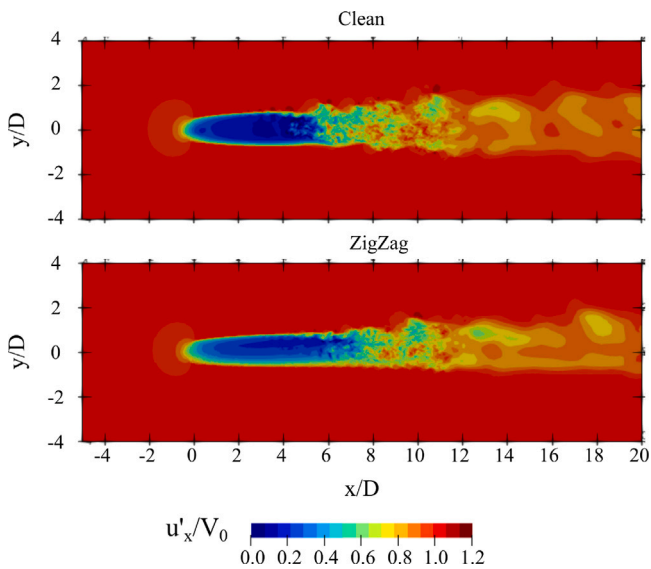


Fig. 18. Contour plots of the normalized instantaneous u'_x/V_0 velocity component in the far wake downstream behind the rotor.

size relative to the blade’s chord length can simulate a case of rather extreme surface contamination. Therefore, the results of this study can be considered as a test for such situations.

- The analysis shows that the differences in the angle of attack estimation are generally small, especially in the upwind section

of the rotor. Higher angles of attack are observed for the S&K database and zigzag configurations, while the clean airfoil has a slightly lower maximum angle of attack. The static maximum lift coefficient is not reached for the measured airfoil characteristics, regardless of the clean or zigzag configurations. The most significant differences in estimating the angle of attack occur in the downwind azimuth range, which is influenced by the velocity field and airfoil characteristics. These differences are primarily caused by the more disturbed velocity field in the clean airfoil case due to the laminar separation bubbles.

- The 2-D CFD results indicate little difference between the turbulence models used, even though the static airfoil characteristics vary between them. The $k-\omega$ SST model produces slightly higher lift coefficients compared to the $\gamma-Re_\theta$ model within the relevant angle of attack range, which explains the minor increase in tangential blade loads. Overall, the flow around the blade should be considered mostly attached, and the laminar separation bubble effects are visible only in the early stages of the rotor cycle.
- The comparison between ALM and 2-D CFD shows that the aerodynamic blade loads are very similar in the upwind part of the rotor but differ more in the downwind section. This difference arises from the 3-D ALM approach considering blade characteristics under low turbulence, whereas the 2-D CFD accounts for local flow conditions. Although 2-D CFD does not capture 3-D effects, existing studies suggest that the actual 3-D aerodynamic loads in the downwind section may be lower than predicted by the 2-D model.
- The nonlinear lift characteristic results from the formation of laminar separation bubbles on the airfoil surface. This leads to a “fuller” and more symmetric aerodynamic wake compared to the case with a linear lift characteristic. The turbulization of the boundary layer also causes the appearance of a small side force acting on the rotor.

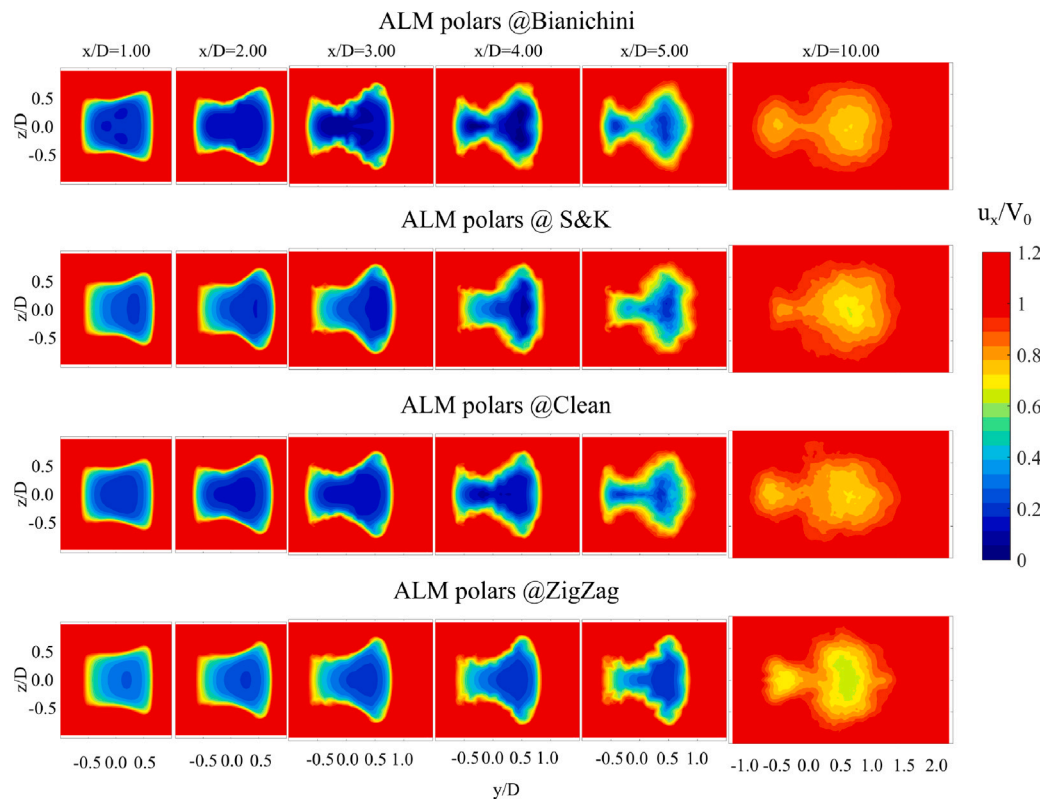


Fig. 19. Contours of normalized streamwise velocity and in-plane velocity fields from 1 to 10 D downstream of the VAWT velocity downstream behind the rotor.

CRedit authorship contribution statement

Krzysztof Rogowski: Writing – review & editing, Writing – original draft, Visualization, Validation, Supervision, Software, Resources, Project administration, Methodology, Investigation, Funding acquisition, Formal analysis, Data curation, Conceptualization. **Jan Michna:** Writing – review & editing, Writing – original draft, Visualization, Validation, Software, Methodology, Formal analysis, Data curation, Conceptualization. **Robert Flemming Mikkelsen:** Writing – review & editing, Writing – original draft, Validation, Methodology, Investigation, Data curation, Conceptualization. **Carlos Simao Ferreira:** Writing – review & editing, Writing – original draft, Supervision, Conceptualization.

Declaration of competing interest

The authors declare that they have no known competing financial interests or personal relationships that could have appeared to influence the work reported in this paper.

Acknowledgments

This research was also conducted with the assistance of the Interdisciplinary Centre for Mathematical and Computational Modeling (ICM) at the University of Warsaw under computational allocations no. G93-1588 and G92-1487.

Data availability

No data was used for the research described in the article.

References

- [1] Tescione G, Ragni D, He C, Simão Ferreira CJ, van Bussel GJW. Near wake flow analysis of a vertical axis wind turbine by stereoscopic particle image velocimetry. *Renew Energy* 2014;70:47–61. <http://dx.doi.org/10.1016/j.renene.2014.02.042>.
- [2] Rezaeiha A, Montazeri H, Blocken B. Towards optimal aerodynamic design of vertical axis wind turbines: Impact of solidity and number of blades. *Energy* 2018;165:1129–48. <http://dx.doi.org/10.1016/j.energy.2018.09.192>.
- [3] Rezaeiha A, Montazeri H, Blocken B. Active flow control for power enhancement of vertical axis wind turbines: Leading-edge slot suction. *Energy* 2019;189:116131. <http://dx.doi.org/10.1016/j.energy.2019.116131>.
- [4] Rogowski K. CFD computation of the H-Darrieus wind turbine—The impact of the rotating shaft on the rotor performance. *Energies* 2019;12(13):2506. <http://dx.doi.org/10.3390/en12132506>.
- [5] Cacciali L, Hansen MOL, Rogowski K. Highly stable lattice Boltzmann method with a 2-D Actuator Line Model for Vertical Axis Wind Turbines. *Energies* 2024;17(19):4847. <http://dx.doi.org/10.3390/en17194847>.
- [6] Lam H, Peng H. Study of wake characteristics of a vertical axis wind turbine by two- and three-dimensional computational fluid dynamics simulations. *Renew Energy* 2016;90:386–98. <http://dx.doi.org/10.1016/j.renene.2016.01.011>.
- [7] Mendoza V, Bachant P, Ferreira C, Goude A. Near-wake flow simulation of a vertical axis turbine using an actuator line model. *Wind Energy* 2019;22(2):171–88. <http://dx.doi.org/10.1002/we.2277>.
- [8] Melani PF, Balduzzi F, Ferrara G, Bianchini A. Tailoring the actuator line theory to the simulation of vertical-axis wind turbines. *Energy Convers Manage* 2021;243:114422. <http://dx.doi.org/10.1016/j.enconman.2021.114422>.
- [9] Castelein D, Tescione G, Ragni D, Simao Ferreira C, Gaunaa M. Creating a benchmark of vertical axis wind turbines in dynamic stall for validating numerical models. In: 33rd Wind energy symposium. AIAA sciTech forum, American Institute of Aeronautics and Astronautics; 2015. <http://dx.doi.org/10.2514/6.2015-0723>.
- [10] Rezaeiha A, Montazeri H, Blocken B. On the accuracy of turbulence models for CFD simulations of vertical axis wind turbines. *Energy* 2019;180:838–57. <http://dx.doi.org/10.1016/j.energy.2019.05.053>.
- [11] Mueller TJ. Fixed and flapping wing aerodynamics for micro air vehicle applications. Reston, VA: American Institute of Aeronautics and Astronautics; 2001. <http://dx.doi.org/10.2514/4.866654>.
- [12] Winslow J, Otsuka H, Govindarajan B, Chopra I. Basic understanding of airfoil characteristics at low Reynolds numbers (104–105). *J Aircr* 2018;55(3):1050–61. <http://dx.doi.org/10.2514/1.C034415>.

- [13] Jacobs EN, Sherman A. Airfoil section characteristics as affected by variations of the Reynolds number. Technical report NACA-TR-586, Langley Field, VA, USA: National Advisory Committee for Aeronautics; 1937, p. 227–67.
- [14] Sheldahl RE, Klimas PC. Aerodynamic characteristics of seven symmetrical airfoil sections through 180-degree angle of attack for use in aerodynamic analysis of vertical axis wind turbines. Technical report SAND-80-2114, Sandia National Lab. (SNL-NM), Albuquerque, NM (United States); 1981, <http://dx.doi.org/10.2172/6548367>.
- [15] Paraschivoiu I. Wind turbine design: with emphasis on Darrieus concept. Presses inter Polytechnique; 2002.
- [16] Rogowski K, Królak G, Bangga G. Numerical study on the aerodynamic characteristics of the NACA 0018 airfoil at low Reynolds number for darrieus wind turbines using the transition SST model. Processes 2021;9(3):477. <http://dx.doi.org/10.3390/pr9030477>.
- [17] Bianchini A, Balduzzi F, Rainbird JM, Peiro J, Graham JMR, Ferrara G, et al. An experimental and numerical assessment of airfoil polars for use in darrieus wind turbines—Part I: Flow curvature effects. J Eng Gas Turbines Power 2015;138(3):032602. <http://dx.doi.org/10.1115/1.4031269>.
- [18] Melani PF, Balduzzi F, Ferrara G, Bianchini A. An annotated database of low Reynolds aerodynamic coefficients for the NACA0018 airfoil. In: AIP conference proceedings, vol. 2191. Erode, India: American Institute of Physics; 2019, 020110. <http://dx.doi.org/10.1063/1.5138843>.
- [19] Gerakopoulos R, Boutilier M, Yarusevych S. Aerodynamic characterization of a NACA 0018 airfoil at low Reynolds numbers. In: 40th Fluid dynamics conference and exhibit. Fluid dynamics and co-located conferences, Chicago, Illinois: American Institute of Aeronautics and Astronautics; 2010, p. 4629. <http://dx.doi.org/10.2514/6.2010-4629>.
- [20] Michna J, Rogowski K. Numerical study of the effect of the Reynolds number and the turbulence intensity on the performance of the NACA 0018 Airfoil at the low Reynolds number regime. Processes 2022;10(5):1004. <http://dx.doi.org/10.3390/pr10051004>.
- [21] Boutilier MS, Yarusevych S. Parametric study of separation and transition characteristics over an airfoil at low Reynolds numbers. Exp Fluids 2012;52:1491–506. <http://dx.doi.org/10.1007/s00348-012-1270-z>.
- [22] Zhang Y, Van Zuijlen A, Van Bussel G. The MEXICO rotor aerodynamic loads prediction: ZigZag tape effects and laminar-turbulent transition modeling in CFD. J Wind Eng Ind Aerodyn 2017;168:152–63. <http://dx.doi.org/10.1016/j.jweia.2017.06.002>.
- [23] Timmer W. Two-dimensional low-Reynolds number wind tunnel results for airfoil NACA 0018. Wind Eng 2008;32(6):525–37. <http://dx.doi.org/10.1260/030952408787548848>.
- [24] Rezaeiha A, Montazeri H, Blocken B. On the accuracy of turbulence models for CFD simulations of vertical axis wind turbines. Energy 2019;180:838–57. <http://dx.doi.org/10.1016/j.energy.2019.05.053>.
- [25] Kruse EK, Sørensen NN, Bak C. Predicting the influence of surface protuberance on the aerodynamic characteristics of a NACA 63₃-418. J Phys: Conf Series 2018;1037:022008. <http://dx.doi.org/10.1088/1742-6596/1037/2/022008>.
- [26] Rogowski K, Mikkelsen RF, Michna J, Wiśniewski J. Aerodynamic performance analysis of NACA 0018 airfoil at low Reynolds numbers in a low-turbulence wind tunnel. Adv Sci Technol Res J 2025;19:136–50. <http://dx.doi.org/10.12913/22998624/195556>.
- [27] Sørensen JN, Shen WZ. Computation of wind turbine wakes using combined Navier-Stokes/actuator-line methodology. In: Proceedings of the 1999 European wind energy conference and exhibition. Nice, France: Routledge; 1999, p. 156–9.
- [28] Bachant P, Goude A, daa-mec, Wosnik M. Turbinesfoam/turbinesfoam: v0.1.1. 2019, <http://dx.doi.org/10.5281/zenodo.3542301>, Version v0.1.1.
- [29] Leishman JG, Beddoes TS. A semi-empirical model for dynamic stall. J Am Helicopter Soc 1989;34(3):3–17. <http://dx.doi.org/10.4050/JAHS.34.3.3>.
- [30] Sheng W, Galbraith RA, Coton FN. Improved Dynamic-Stall-Onset criterion at low Mach numbers. J Aircr 2007;44(3):1049–52. <http://dx.doi.org/10.2514/1.29163>.
- [31] Dyachuk E, Goude A, Bernhoff H. Dynamic stall modeling for the conditions of vertical axis wind turbines. AIAA J 2014;52(1):72–81. <http://dx.doi.org/10.2514/1.J052633>.
- [32] Mendoza V, Bachant P, Wosnik M, Goude A. Validation of an actuator line model coupled to a dynamic stall model for pitching motions characteristic to vertical axis turbines. J Phys Conf Ser 2016;753(2):022043. <http://dx.doi.org/10.1088/1742-6596/753/2/022043>.
- [33] Bachant P, Goude A, Wosnik M. Actuator line modeling of vertical-axis turbines. 2018, <http://dx.doi.org/10.48550/arXiv.1605.01449>, arXiv, URL <https://arxiv.org/abs/1605.01449>, arXiv:1605.01449.
- [34] Nordlund M, Stanic M, Kuczaj A, Frederix E, Geurts B. Improved PISO algorithms for modeling density varying flow in conjugate fluid–porous domains. J Comput Phys 2016;306:199–215. <http://dx.doi.org/10.1016/j.jcp.2015.11.035>.
- [35] Huang M. Wake and wind farm aerodynamics of vertical axis wind turbines [Ph.D. thesis], Delft University of Technology; 2023, <http://dx.doi.org/10.4233/uuid:14619578-e44f-45bb-a213-a9d179a54264>.
- [36] Rogowski K, Michna J, Ferreira CS. Numerical analysis of aerodynamic performance of a fixed-pitch Vertical Axis Wind Turbine rotor. Adv Sci Technol Res J 2024;18(6):97–109. <http://dx.doi.org/10.12913/22998624/191128>.
- [37] Rezaeiha A, Kalkman I, Blocken B. CFD simulation of a vertical axis wind turbine operating at a moderate tip speed ratio: Guidelines for minimum domain size and azimuthal increment. Renew Energy 2017;107:373–85. <http://dx.doi.org/10.1016/j.renene.2017.02.006>.
- [38] ANSYS fluent theory guide, release 2023 R2. ANSYS Inc.; 2023.
- [39] Melani PF, Balduzzi F, Brandetti L, Ferreira CS, Bianchini A. An experimental and numerical analysis of the dynamic variation of the angle of attack in a vertical-axis wind turbine. J Phys Conf Ser 2020;1618(5):052064. <http://dx.doi.org/10.1088/1742-6596/1618/5/052064>.
- [40] Mendoza V. Aerodynamic studies of vertical axis wind turbines using the actuator line model. [Ph.D. thesis], Uppsala, Sweden: Uppsala: Acta Universitatis Upsaliensis; 2018.
- [41] Bianchini A, Balduzzi F, Rainbird JM, Peiro J, Graham JMR, Ferrara G, et al. An experimental and numerical assessment of airfoil polars for use in darrieus wind turbines—Part II: Post-stall data extrapolation methods. J Eng Gas Turbines Power 2015;138(3):032602. <http://dx.doi.org/10.1115/1.4031269>.
- [42] Huang M, Ferreira C, Sciacchitano A, Scarano F. Wake scaling of actuator discs in different aspect ratios. Renew Energy 2022;183:866–76. <http://dx.doi.org/10.1016/j.renene.2021.11.045>.